Homogenization Modeling for Mechanical Properties of Composite Conductor With Cooling Channel

by Wei Sun and Jerome T. Tzeng

20030106 044

NOTICES

Disclaimers

Army Research Laboratory
Aberdeen Proving Ground, MD 21005-5069

Homogenization Modeling for Mechanical Properties of Composite Conductor With Cooling Channel

Wei Sun and Jerome T. Tzeng
Weapons and Materials Research Directorate, ARL

Abstract

An electrical composite conductor may consist of a metallic core with a cooling channel and a multilayered insulating material. A model was developed to predict the mechanical properties of the composite conductor based on two-level homogenization hierarchies. A composite cylinder assembly model was developed in the level 1 homogenization for metallic core with a cooling channel, in which the cooling channel was analogized as a fiber void with null material properties. The effective mechanical properties of the composite insulation layers were homogenized by smearing the properties of the multiple polymer coatings and fiber-reinforced composite. In the level 2 homogenization, combined homogenization sequences were used based on the requirement of the displacement- or the traction-prescribed continuity. The developed model can calculate the nine effective mechanical constants of the conductor made of a metallic core and any angle ($\pm\theta°$) plain-woven glass-fiber composite. The model predictions were compared well with the results obtained from the finite element analyses. The developed model provides a theoretical basis and an accurate calculation for effective mechanical constants that are often difficult to be accurately determined through an experimental approach due to the structural heterogeneity and material anisotropy of the composite conductor.

Contents

INTENTIONALLY LEFT BLANK.

List of Figures

INTENTIONALLY LEFT BLANK.

List of Tables

INTENTIONALLY LEFT BLANK.

1. Introduction

Electrical machinery, which ranges from electric drive vehicles to the electric launch system, is considered to be one of the most important components in the future combat systems. Compact, durable, and highly mobile power generators and motors are necessary for the success of all electrical systems [1, 2]. Extensive research has been conducted for electromagnetic (EM) structural design, analysis, and mechanics on various technical areas [3–9]. Because of the complex geometry and the heterogeneity of the conductor with insulation layers, the EM systems usually need to be analyzed using numerical techniques such as the finite element method. However, a conventional finite element analysis (FEA) cannot analyze each structural entity from the whole EM system because of the limit of computational time and machine capacity limitations. Therefore, the EM structure must be analyzed separately at different levels, i.e., a global and local level. The analyses conducted at the global level use the homogenized effective properties derived from the representative volume element, or a unit cell of the EM conductor [10, 11]. At this level, the structure of the composite conductor is homogenized by smearing the distinctive phases of the constituents, and the effective properties of the EM conductor unit cell are derived. The unit cell properties are used to predict the global responses of the EM system subjected to a given loading condition. The results derived from the global analysis will then be used in the local level analysis where the individual constituents, including their geometries and properties, are considered, and the detail stress and deformation will be calculated. Clearly, an accurate prediction of the conductor effective mechanical properties is critical because they provide the fundamental material parameters in the design and analysis of the EM structural behavior under the combined mechanical, EM, and thermal loading, as well as the system structural integrity, insulation, and service life.

In this report, a homogenization modeling to predict the effective mechanical properties of EM composite conductor consisting of metallic core with cooling channel and multilayered insulating materials is presented. The model was developed based on the two-level homogenization hierarchy schemes, in conjunction with the composite cylinder assembly model (CCAM) and the combined homogenization sequences. The developed model was applied to predict the effective properties of the EM conductor made of metallic conducting core with cooling channel, insulation layers of different phase materials, and ±θ° plain-woven glass-fiber composite. These effective properties are composed of nine material constants that are often difficult to accurately determine through an experimental approach due to the structural heterogeneity and material anisotropy. The model predictions were also compared and validated with finite element calculation.

The presentation of this report is organized as follows: Section 2 describes the conductor schematics, including its structural layout, geometric and material configuration, as well as the

homogenization scheme used in the study; the analytical model to predict the conductor homogenized effective constants is derived and presented in section 3; the application of the model to predict the effective properties, the results, and comparisons will be presented in section 4; a summary and conclusion follows in section 5.

2. Conductor Structural Layout and Homogenization Scheme

We consider a composite conductor consisting of an interior metallic conducting core with cooling channel and the exterior insulation layers made by different insulation materials and $\pm\theta°$ plain-woven glass-fiber-reinforced composite. The metallic core conducts pulsating EM currents that can cause rapid heating of the core material. The fiber-reinforced composite is used to provide desired mechanical and thermal properties, as well as an extra insulating protection. The small cooling channel in the middle of the core lets a pressurized coolant circulate at a high velocity in order to reduce the heat. The metallic conductor core with cooling channel, wrapped with the insulating composites, is packed into a winding assembly. A schematic representation of the constituent materials and geometries for such a composite conductor unit cell is presented in Figure 1.
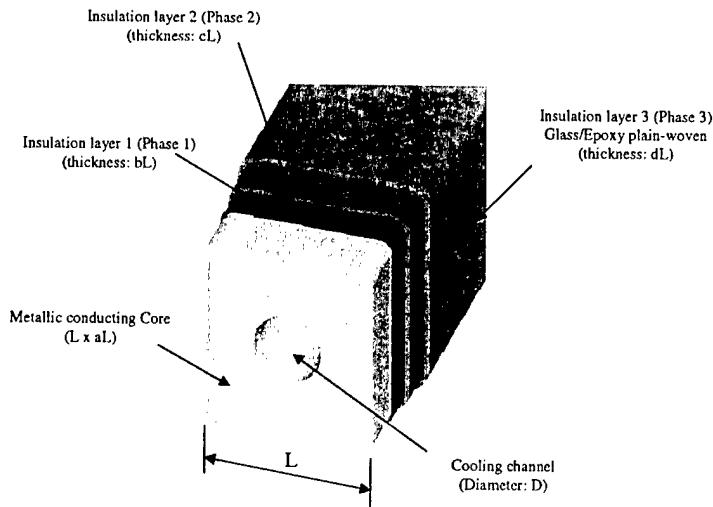

Figure 1. Schematic representation of a composite conductor unit cell.

For a composite conductor unit cell as shown in Figure 1, we used the following two-level homogenization schemes to derive its effective mechanical properties:

Level 1: Homogenization for effective metallic core and effective insulation composite blocks;

2

Level 2: Homogenization for effective composite conductor consisting of effective metallic core and effective insulation composite blocks.

The level 1 homogenization is composed of two separate procedures: to determine the effective mechanical properties of metallic conducting core with cooling channel through composite cylinder assembly model [12] and to determine the effective mechanical properties of the insulation layer, which consists of different phase insulation materials and glass composite. The results of the homogenized mechanical properties of the insulation layers and the metallic conducting core calculated from the level 1 homogenization will be used to derive the effective mechanical properties of the composite conductor in the level 2 homogenization. The homogenization scheme is illustrated in Figure 2, and the detail derivation is presented in the next section.
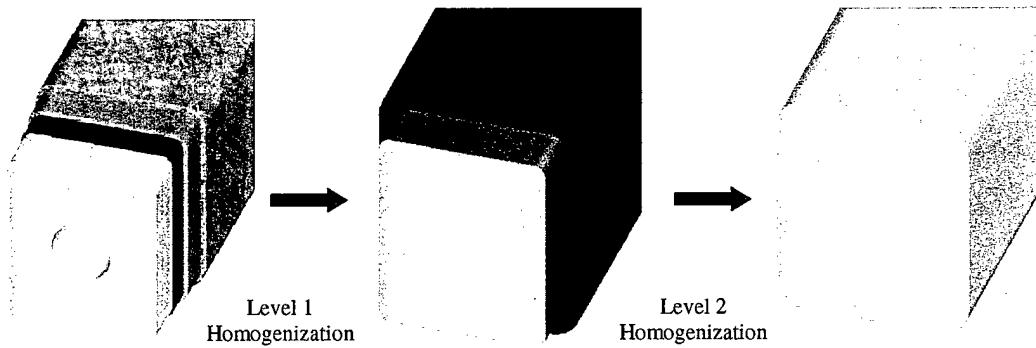
Figure 2. Two-level homogenization scheme.

3. Homogenization Modeling

3.1 Homogenization of the Effective Metallic Core With Cooling Channel

We analogize the metallic core containing cooling channel in Figure 3 as a composite cylinder assembly, which is composed of a matrix (metallic core) and a cylindrical fiber (cooling channel as void). For this type of composite assembly, we apply a CCAM [12] to calculate its homogenized mechanical properties.

As shown in the derivation of the CCAM [12], the effective mechanical constants of the conducting core containing a cooling channel can be expressed by

$$E_A^M = E_1 V_1 + E_2 V_2 + \frac{4(v_2 - v_1)^2 V_1 V_2}{\dfrac{V_1}{k_2} + \dfrac{V_2}{k_1} + \dfrac{1}{G_1}} ; \tag{1}$$

3

Figure 3. Effective modeling of metallic core with cooling channel by CCAM.

$$v_A^M = v_1 V_1 + v_2 V_2 + \frac{(v_2 - v_1)(\frac{1}{k_1} - \frac{1}{k_2})V_1 V_2}{\frac{V_1}{k_2} + \frac{V_2}{k_1} + \frac{1}{G_1}} \ ; \tag{2}$$

$$G_A^M = G_1 \frac{G_1 V_1 + G_2(1 + V_2)}{G_1(1 + V_2) + G_2 V_1} \ ; \tag{3}$$

$$G_T^M = \frac{G_{T(+)}^M + G_{T(-)}^M}{2} \ ; \tag{4}$$

$$E_T^M = \frac{(\frac{4k^M G_{T(+)}^M}{k^M + mG_{T(+)}^M}) + (\frac{4k^M G_{T(-)}^M}{k^M + mG_{T(-)}^M})}{2} \ ; \tag{5}$$

$$v_T^M = \frac{k^M - mG_T^M}{k^M + mG_T^M} \ ; \tag{6}$$

with

$$G_{T(+)}^M = G_1 \frac{(1 + \alpha V_2^3)(\frac{G_2 + G_1 \beta}{G_2 - G_1} + \beta V_2) - 3v_2 V_1^2 \beta^2}{(1 + \alpha V_2^3)(\frac{G_2 + G_1 \beta}{G_2 - G_1} - V_2) - 3V_2 V_1^2 \beta^2} \ ; \tag{7}$$

$$G_{T(-)}^M = G_1[1 + \frac{V_2}{\frac{G_1}{G_2 - G_1} + \frac{V_1}{1 + \beta}}] \ ; \tag{8}$$

4

$$\alpha = \frac{\dfrac{G_1}{3-4v_1} - \dfrac{G_2}{3-4v_2}}{G_1 + \dfrac{G_2}{3-4v_2}};$$ (9)

$$\beta = \frac{1}{3-4v_1};$$ (10)

$$k^M = k_1 + \frac{V_2}{\dfrac{1}{k_2 - k_1} + \dfrac{V_1}{k_1 + G_1}};$$ (11)

$$m = 1 + \frac{4k^M (v_A^M)^2}{E_A^M}.$$ (12)

The nomenclatures used in equations (1)–(12) are defined as follows: superscript M denotes metallic core; subscripts A and T denote the effective properties in the channel axial direction (in Z direction) and in the transverse direction (in X or Y direction), respectively; T(+) and T(−) stand for the upper and lower bounds; 1 and 2 stand for homogenized metallic core, original metallic core, and cooling channel (fiber); E is for Young's modulus; G is for shear modulus; k is for bulk modulus; υ is for Poisson's ratio, and V is for volume fraction.

If we analogize the cooling channel as a cylindrical void in the CCAM as shown in Figure 3, E_2, G_2, k_2, and υ_2 will be equal to zero. Substituting these values into equations (1)–(12) obtain

$$E_A^M = E_1 V_1 = E_1(1 - V_2),$$ (13)

$$v_A^M = v_1,$$ (14)

$$G_A^M = G_1 \frac{(1 - V_2)}{(1 + V_2)},$$ (15)

$$\alpha = \beta = \frac{1}{3 - 4v_1},$$ (16)

$$k^M = \frac{k_1 G_1 (1 - V_2)}{G_1 + k_1 V_2},$$ (17)

with the transverse constants being defined by equations (4)–(8).

3.2 Homogenization of the Insulation Layers as Composite Blocks

Because of the different fiber orientations in the plain-woven composite with respect to the global conductor coordinate system, we homogenize the over-wrapped insulation layers as two different composite blocks: CB1 at the horizontal surfaces of the conducting core and CB2 at the vertical surfaces. The difference between CB1 and CB2 is in the fiber orientation of the

plain-woven composite with respect to the global coordinate system XYZ, as indicated in Figure 4. The detail section views of the insulation composite block CB1 and CB2 are shown in Figure 4b and Figure 4c, and the relationship between the local composite coordinate system xyz for a typical insulation composite block and the conductor global structural coordinate system XYZ is shown in Figure 4d, respectively.
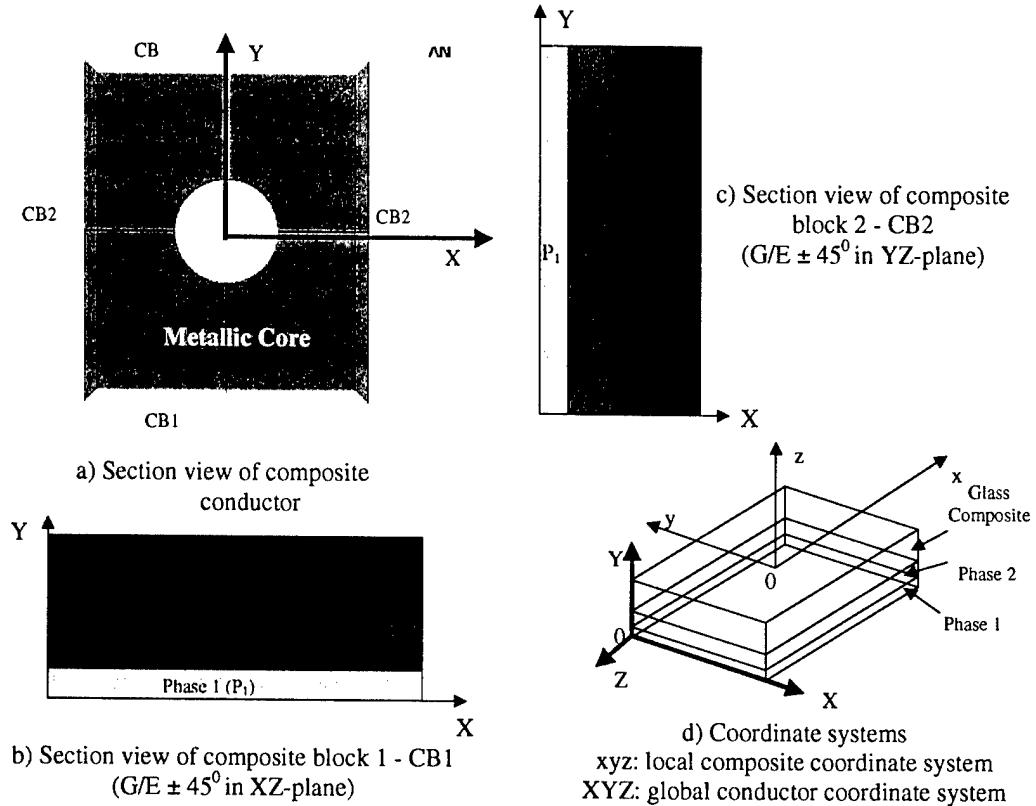
Figure 4. Section views of conductor and insulation composite blocks.

Based on the composite mechanics and homogenization theory [14–16], we can derive an analytical expression for elastic constants of the typical composite block shown in Figure 4d. Its nine elastic constants in the global coordinate system XYZ can be expressed in terms of the elastic constants of its constituent layers and their volume fractions as:

$$E_{XX}^{CB} = V_{P_1} E_{P_1} + V_{P_2} E_{P_2} + V_G E_{yy}^G ; \qquad (18)$$

$$E_{YY}^{CB} = \frac{E_{P_1} E_{P_2} E_{zz}^G}{V_{P_1} E_{P_2} E_{zz}^G + V_{P_2} E_{P_1} E_{zz}^G + V_G E_{P_1} E_{P_2}} ; \qquad (19)$$

$$E_{ZZ}^{CB} = V_{P_1} E_{P_1} + V_{P_2} E_{P_2} + V_G E_{xx}^G ; \qquad (20)$$

$$v_{XY}^{CB} = v_{XY}^{CB} = V_{P_1} v_{P_1} + V_{P_2} v_{P_2} + V_G v_{yz}^G ; \qquad (21)$$

6

$$G_{XY}^{CB} = \frac{G_{P_1} G_{P_2} G_{yz}^G}{V_{P_1} G_{P_2} G_{yz}^G + V_{P_2} G_{P_1} G_{yz}^G + V_G G_{P_2} G_{P_1}} \; ; \qquad (22)$$

$$G_{YZ}^{CB} = \frac{G_{P_1} G_{P_2} G_{xz}^G}{V_{P_1} G_{P_2} G_{xz}^G + V_{P_2} G_{P_1} G_{xz}^G + V_G G_{P_2} G_{P_1}} \; ; \qquad (23)$$

$$G_{XZ}^{CB} = V_{P_1} G_{P_1} + V_{P_2} G_{P_2} + V_G G_{xy}^G \; ; \qquad (24)$$

$$v_{YZ}^{CB} = V_{P_1} v_{P_1} + V_{P_2} v_{P_2} + V_G v_{xz}^G \; ; \qquad (25)$$

$$v_{XZ}^{CB} = \frac{v_{P_1} v_{P_2} v_{xy}^G}{V_{P_1} v_{P_2} v_{xy}^G + V_{P_2} v_{P_1} v_{xy}^G + V_G v_{P_1} v_{P_2}} \; . \qquad (26)$$

The elastic constants of the plain-woven glass/epoxy composite in the local coordinate system (xyz) can be determined by

$$E_{xx}^G = \frac{E_{11} E_{22}}{E_{22} \cos^4 \theta + E_{11} E_{22} (\frac{1}{G_{12}} - \frac{2 v_{12}}{E_{11}}) \sin^2 \theta \cos^2 \theta + E_{11} \sin^4 \theta} \; ; \qquad (27)$$

$$E_{yy}^G = \frac{E_{11} E_{22}}{E_{11} \cos^4 \theta + E_{11} E_{22} (\frac{1}{G_{12}} - \frac{2 v_{12}}{E_{11}}) \sin^2 \theta \cos^2 \theta + E_{22} \sin^4 \theta} \; ; \qquad (28)$$

$$v_{xy}^G = E_{xx} [\frac{v_{12}}{E_{11}} (\sin^4 \theta + \cos^4 \theta) - (\frac{1}{E_{11}} + \frac{1}{E_{22}} - \frac{1}{G_{12}}) \sin^2 \theta \cos^2 \theta] \; ; \qquad (29)$$

$$G_{xy}^G = \frac{G_{12}}{2 G_{12} (\frac{2}{E_{11}} + \frac{2}{E_{22}} + \frac{4 v_{12}}{E_{11}} - \frac{1}{G_{12}}) \sin^2 \theta \cos^2 \theta + (\sin^4 \theta + \cos^4 \theta)} \; ; \qquad (30)$$

$$G_{yz}^G = G_{23} = \frac{0.5 [V_f + V_m \times 0.5 (1 + \frac{E_m}{E_f})]}{[V_f (\frac{1}{E_f} + \frac{v_f}{E_f}) + V_m \times 0.5 (1 + \frac{E_m}{E_f}) (\frac{1}{E_m} + \frac{v_m}{E_m})]} \; ; \qquad (31)$$

$$E_{zz}^G = E_{33} = \frac{E_f E_m}{V_f E_m + V_m E_f} \; ; \qquad (32)$$

$$v_{yz}^G = v_{23} = V_f v_f + V_m v_m \; ; \qquad (33)$$

$$v_{xz}^G = v_{13} = V_f v_f + V_m v_m \; ; \qquad (34)$$

7

$$G_{xz}^{G} = G_{13} = \frac{0.5[V_f + V_m \times 0.5(1 + \frac{E_m}{E_f})]}{[V_f(\frac{1}{E_f} + \frac{v_f}{E_f}) + V_m \times 0.5(1 + \frac{E_m}{E_f})(\frac{1}{E_m} + \frac{v_m}{E_m})]}. \tag{35}$$

The detail derivation for glass composite mechanical properties have been addressed by Sun and Tzeng [10], and Huang [13]. The additional nomenclatures in equations (18)–(35), as well as in the following expressions, are defined as follows: the superscripts CB1 and CB2 denote composite blocks 1 and 2; the subscripts 1, 2, and 3 are for the composite principle coordinate system; x, y, or z denote components in the composite local coordinate system; X, Y, and Z denote the conductor global structural coordinate system; P_1, P_2, and G denote phase 1, phase 2, and glass composite insulation materials; the subscripts f and m denote constituent fiber and matrix in glass composite materials; V_{Pj}^{i} denotes the volume fraction of individual insulation material in the composite blocks, with i = 1, 2 for CB1 and CB2, and j = 1, 2, 3 for phase 1, phase 2, and phase 3 material, respectively; and V_f and V_m denote the volume fraction of the fiber and matrix in glass composites.

From equations (18)–(26), we can determine the effective elastic constants for composite blocks CB1 and CB2 as shown in Figures 4b and 4c. Their relations to the constants of the typical composite block (Figure 4d) are:

$$\begin{aligned}
E_{XX}^{CB1} &= E_{XX}^{CB}; & E_{YY}^{CB1} &= E_{YY}^{CB}; & E_{ZZ}^{CB1} &= E_{ZZ}^{CB} \\
G_{XY}^{CB1} &= G_{XY}^{CB}; & G_{YZ}^{CB1} &= G_{YZ}^{CB}; & G_{XZ}^{CB1} &= G_{XZ}^{CB} \\
\upsilon_{XY}^{CB1} &= \upsilon_{XY}^{CB}; & \upsilon_{YZ}^{CB1} &= \upsilon_{YZ}^{CB}; & \upsilon_{XZ}^{CB1} &= v_{XZ}^{CB}
\end{aligned} \tag{36}$$

for composite block CB1, and

$$\begin{aligned}
E_{XX}^{CB2} &= E_{YY}^{CB}; & E_{YY}^{CB2} &= E_{XX}^{CB}; & E_{ZZ}^{CB2} &= E_{ZZ}^{CB} \\
G_{XY}^{CB2} &= G_{XY}^{CB}; & G_{YZ}^{CB2} &= G_{XZ}^{CB}; & G_{XZ}^{CB2} &= G_{YZ}^{CB} \\
\upsilon_{XY}^{CB2} &= \upsilon_{XY}^{CB}; & \upsilon_{YZ}^{CB2} &= \upsilon_{XZ}^{CB}; & \upsilon_{XZ}^{CB2} &= v_{YZ}^{CB}
\end{aligned} \tag{37}$$

for composite block CB2.

3.3 Homogenization of EM Composite Conductor

Homogenization for effective mechanical properties of the composite conductor is accomplished by homogenizing the effective metallic conducting core with the composite insulation blocks. The schematic of the homogenization is illustrated in Figure 5.

To homogenize the mechanical properties of the composite conductor, we consider using a two-sequence model as shown in Figure 6. Namely, the homogenized mechanical properties of the composite conductor are determined through a combined sequence operations. In sequence 1, we first homogenize the insulation composite block and the metallic conducting core to

8
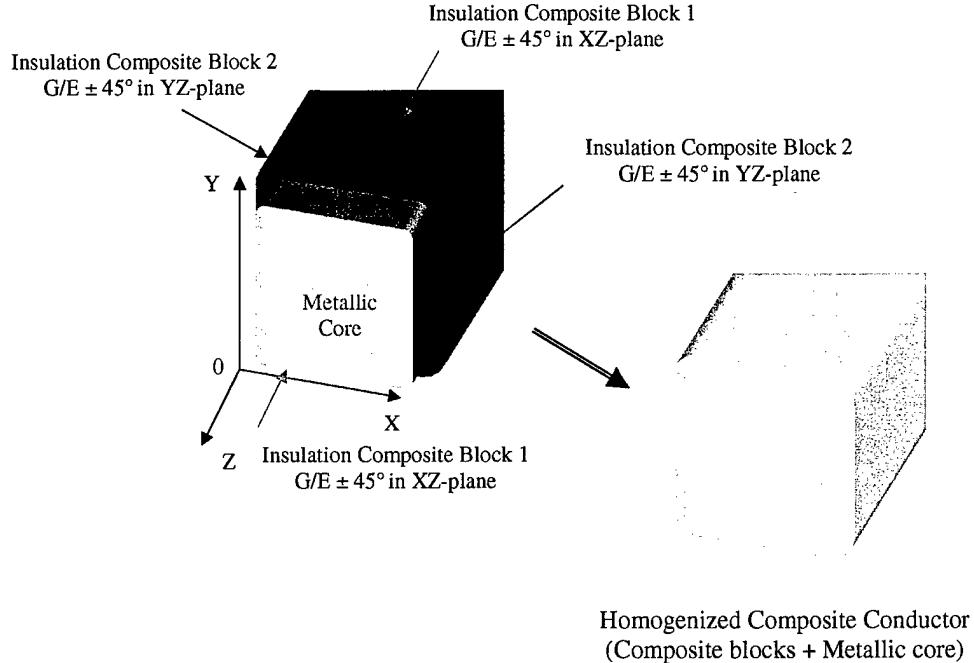
Figure 5. Homogenization of composite conductor.

a) $E_{ij}^{CC} = \{E_{ij}^{CB1}, E_{ij}^{CB2-M}\}$

b) $E_{ij}^{CC} = \{E_{ij}^{CB2}, E_{ij}^{CB1-M}\}$
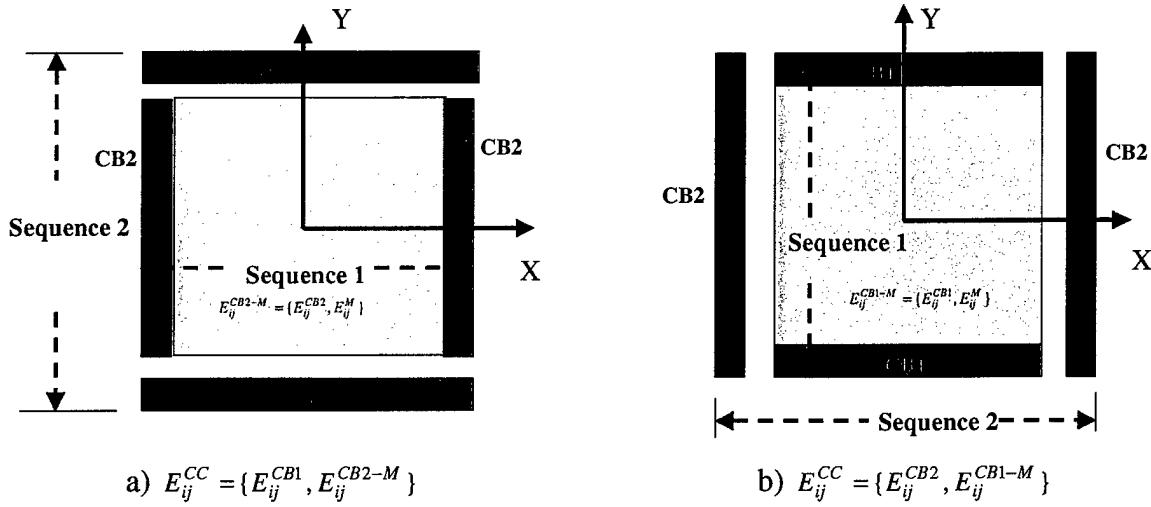
Figure 6. Combined sequences for composite conductor homogenization.

determine the effective mechanical properties E_{ij}^{CB2-M} (Figure 6a) or E_{ij}^{CB1-M} (Figure 6b). In sequence 2, we add the remaining insulation composite blocks to the results of the sequence 1 homogenization to derive the effective mechanical properties of the composite conductor E_{ij}^{CC}.

Depending on the responses of the constituents to the prescribed deformation, the effective constants derived from the sequence operations $E_{ij}^{CBi-M} = \{(E_{ij}^{CBi}, E_{ij}^{M}), i = 1,2\}$ or $E_{ij}^{CC} = \{(E_{ij}^{CBi}, E_{ij}^{CBi-M}), i = 1,2\}$ will be calculated either through a displacement-prescribed relation:

9

$$E_{ij}^{effective} = V^1 E_{ij}^1 + V^2 E_{ij}^2 + \ldots \tag{38}$$

or a stress-prescribed relation:

$$E_{ij}^{effective} = \frac{E_{ij}^1 E_{ij}^2 \ldots}{V^1 E_{ij}^2 + V^2 E_{ij}^1 + \ldots}. \tag{39}$$

Based on the previously mentioned analogies, we establish the following mathematical formulations to calculate the homogenized mechanical properties of the composite conductor:

$$E_{XX}^{CC} = V^{CB1} E_{XX}^{CB1} + \frac{E^M E_{XX}^{CB2}}{V^{CB2} E^M + V^M E_{XX}^{CB2}}; \tag{40}$$

$$E_{YY}^{CC} = V^{CB2} E_{YY}^{CB2} + \frac{E^M E_{YY}^{CB1}}{V^{CB1} E^M + V^M E_{YY}^{CB1}}; \tag{41}$$

$$E_{ZZ}^{CC} = V^M E^M + V^{CB1} E_{ZZ}^{CB1} + V^{CB2} E_{ZZ}^{CB2}; \tag{42}$$

$$G_{XY}^{CC} = \frac{G_{XY}^{CB1} G_{XY}^{CB2} G^M}{G_{XY}^{CB2} G^M V^{CB1} + (V^{CB2} + V^M) G_{XY}^{CB1} (V^{CB2} G^M + V^M G_{XY}^{CB2})}; \tag{43}$$

$$G_{YZ}^{CC} = \frac{G_{YZ}^{CB1} (V^{CB1} G_{YZ}^{CB2} + V^M G^M)}{(V^{CB2} + V^M) G_{YZ}^{CB1} + V^{CB1} (V^{CB2} G_{YZ}^{CB2} + V^M G^M)}; \tag{44}$$

$$G_{XZ}^{CC} = \frac{G_{XZ}^{CB2} (V^{CB1} G_{XZ}^{CB1} + V^M G^M)}{(V^{CB1} + V^M) G_{XZ}^{CB2} + V^{CB2} (V^{CB2} G_{XZ}^{CB1} + V^M G^M)}; \tag{45}$$

$$v_{XY}^{CC} = V^{CB1} v_{XY}^{CB1} + \frac{v^M v_{XY}^{CB2}}{V^{CB2} v^M + V^M v_{XY}^{CB2}}; \tag{46}$$

$$v_{YZ}^{CC} = \frac{v^M v_{YZ}^{CB1} v_{YZ}^{CB2}}{V^{CB1} v_{YZ}^{CB2} v^M + V^{CB2} v_{YZ}^{CB1} v^M + V^M v_{YZ}^{CB1} v_{YZ}^{CB2}}; \tag{47}$$

$$v_{XZ}^{CC} = \frac{v^M v_{XZ}^{CB1} v_{XZ}^{CB2}}{V^{CB1} v_{XZ}^{CB2} v^M + V^{CB2} v_{XZ}^{CB1} v^M + V^M v_{XZ}^{CB1} v_{XZ}^{CB2}}. \tag{48}$$

In equations (40)–(48), the homogenized mechanical properties of metallic conducting core are determined by the CCAM model and are related to the global coordinate system as:

$$E_{XX}^M = E_{YY}^M = E_T^M, \ E_{ZZ}^M = E_A^M;$$

$$G_{XY}^M = G_T^M, \ G_{XZ}^M = G_{YZ}^M = G_A^M; \tag{49}$$

$$v_{XY}^M = v_T^M, \ v_{XZ}^M = v_{YZ}^M = v_A^M.$$

4. Results and Comparisons

4.1 Results of the Modeling Prediction

The assumed constituent material properties and the designed geometry in the conductor unit cell (Figure 1) are listed in Table 1.

Table 1. Assumed constituent material properties and geometries.

Constituent Material	Dimension	Material Properties
Metallic Conducting Core	Width × height × depth (L × aL × L)	Young's modulus E_M: 10.0 (10^6 psi) Poisson's ratio υ_M: 0.32 Diameter of cooling channel: D
Phase 1 Insulation Material	Thickness bL	Young's modulus E_{P1}: 0.5 (10^6 psi) Poisson's ratio υ_{P1}: 0.35
Phase 2 Insulation Material	Thickness cL	Young's modulus E_{P2}: 0.075 (10^6 psi) Poisson's ratio υ_{P2}: 0.35
Phase 3 Glass/Epoxy Composite	Thickness dL ±45° plain woven	E-glass fiber: E_f: 10.5 (10^6 psi); υ_f: 0.22 Epoxy: E_m: 0.5 (10^6 psi); υ_m: 0.35 Fiber volume fraction V_f: 0.5

From the equations defined in the level 1 and level 2 homogenization, we obtain the following homogenized elastic material constants for metallic conducting core with the cooling channel, for composite insulation blocks, and for composite conductor. These results are summarized in Table 2.

Table 2. Homogenized elastic mechanical constants (L = 1 in, a = 1.5, b = c = d = 0.02, D = 0.3 in).

Homogenized Conductor Core	Composite Block CB1	Composite Block CB2	Composite Conductor
E^M_A = 8.115 Mpsi E^M_T = 6.252 Mpsi G^M_A = 2.586 Mpsi G^M_T = 2.424 Mpsi υ^M_A = 0.320 υ^M_T = 0.290	E^{CB1}_{XX} = 0.675 Mpsi E^{CB1}_{YY} = 0.183 Mpsi E^{CB1}_{ZZ} = 0.675 Mpsi G^{CB1}_{XY} = 0.069 Mpsi G^{CB1}_{YZ} = 0.069 Mpsi G^{CB1}_{XZ} = 0.417 Mpsi υ^{CB1}_{XY} = 0.089 υ^{CB1}_{YZ} = 0.328 υ^{CB1}_{XZ} = 0.378	E^{CB2}_{XX} = 0.183 Mpsi E^{CB2}_{YY} = 0.675 Mpsi E^{CB2}_{ZZ} = 0.675 Mpsi G^{CB2}_{XY} = 0.069 Mpsi G^{CB2}_{XZ} = 0.417 Mpsi G^{CB2}_{YZ} = 0.069 Mpsi υ^{CB2}_{XY} = 0.328 υ^{CB2}_{YZ} = 0.378 υ^{CB2}_{XZ} = 0.328	E^{CC}_{XX} = 1.485 Mpsi E^{CC}_{YY} = 2.011 Mpsi E^{CC}_{ZZ} = 6.826 Mpsi G^{CC}_{XY} = 0.368 Mpsi G^{CC}_{YZ} = 0.694 Mpsi G^{CC}_{XZ} = 0.522 Mpsi υ^{CC}_{XY} = 0.322 υ^{CC}_{YZ} = 0.326 υ^{CC}_{XZ} = 0.324

4.2 Comparison With the Numerical (Finite Element) Solution

The finite element model is developed based on the designed computer-aided design (CAD) geometry. The FEA software used in the analysis is ANSYS 5.6.3. A total of 6300 8-node brick

elements was generated in ANSYS for the unit cell CAD model. Out of the 6300 elements, there are 1260 8-node Solid64-type structural anisotropic elements in CB1, 1440 8-node Solid64-type structural anisotropic elements in CB2, and 3600 8-node Solid45-type structural brick elements in the metallic core. The material properties of CB1 and CB2 are determined from the equations derived in section 3. The FEA mesh, loading, and boundary condition for determining E_{XX}^{CC} is presented in Figure 7. For the purpose of description, we present only one case of determining the effective constant E_{XX}^{CC} by using the FEA model and numerical calculation. A description of using the FEA model and numerical approach to calculate all nine mechanical constants was detailed by Hashin [12].
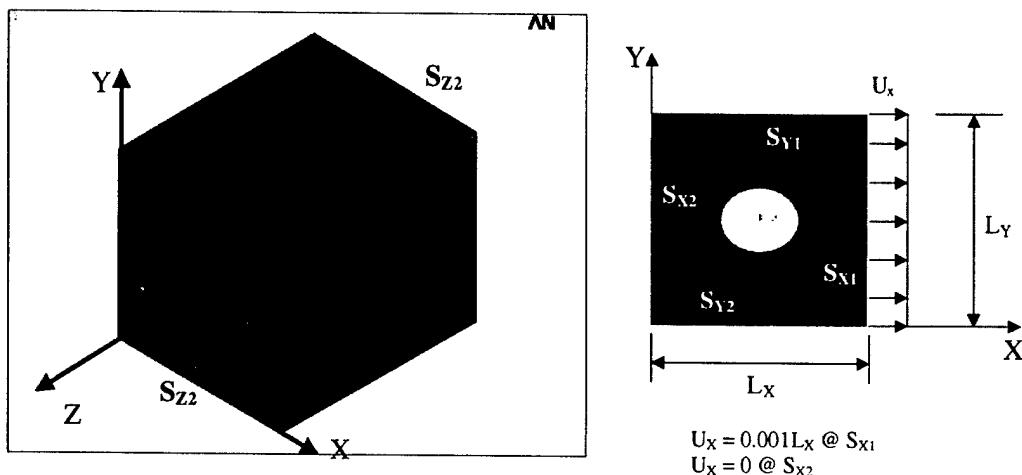
Figure 7. FEA mesh, loading, and boundary condition for determining E_{XX}^{CC}.

Based on the prescribed loading and boundary condition as shown in Figure 7, the conductor effective constant E_{XX}^{CC} can be determined as

$$E_{XX}^{CC} = \frac{\sigma_X}{\varepsilon_X} = \frac{(\frac{R_X}{A_{SX2}})}{(\frac{U_X}{L_X})} = 0.001 \times \frac{R_X}{A_{SX2}}, \tag{50}$$

and

$$R_X = \int_{S_{X_2}} N_X dA, \tag{51}$$

with

$$U_X = 0.001 L_X \text{ on } S_{X1}, \tag{52}$$

$$U_X = 0.0 \text{ on } S_{X2}, \tag{53}$$

12

where U_x is the prescribed displacement on the surface S_{X1} and S_{X2}; A_{SX1} and A_{SX2} are the areas of the surface S_{X1} and S_{X2}, respectively; L_X is the dimension of the unit cell in the X direction; a scale of 0.001 in the application displacement on the surface S_{X1} produces a uniform strain at the value of 0.1%, and R_X is the X-component of the average reaction force produced on the surface S_{X2} as a result of the prescribed displacement U_X on the surface S_{X1}.

Comparisons of the analytical predictions to the numerical calculations based on the FEA are presented in Figures 8 and 9 for the composite conductor with different core cross sections. It can be seen that the mechanical constants predicted from the analytical model agree well with the finite element predictions for both cases, except for a slight difference between the predictions of the in-plane Poisson's ratio υ_{xy}.
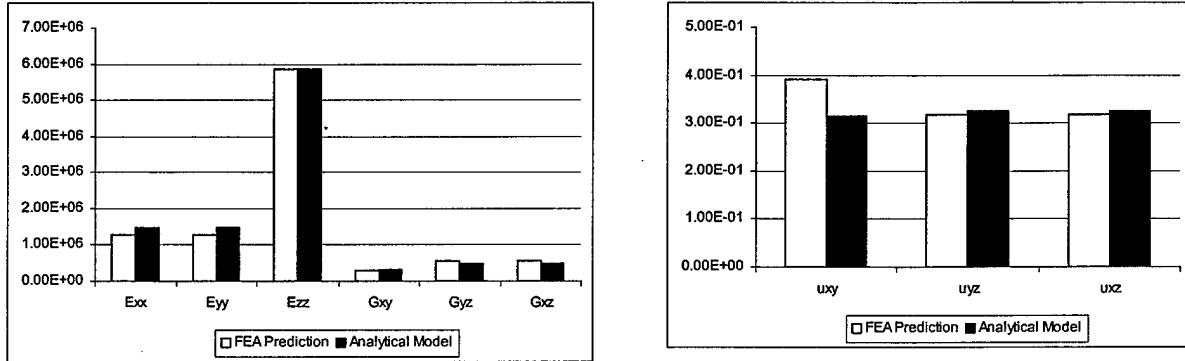
Figure 8. Comparison of FEA and analytical predictions (conducting core with cross section: 1 × 1 in, insulation layer thickness: 0.02 in, D = 0.3 in).
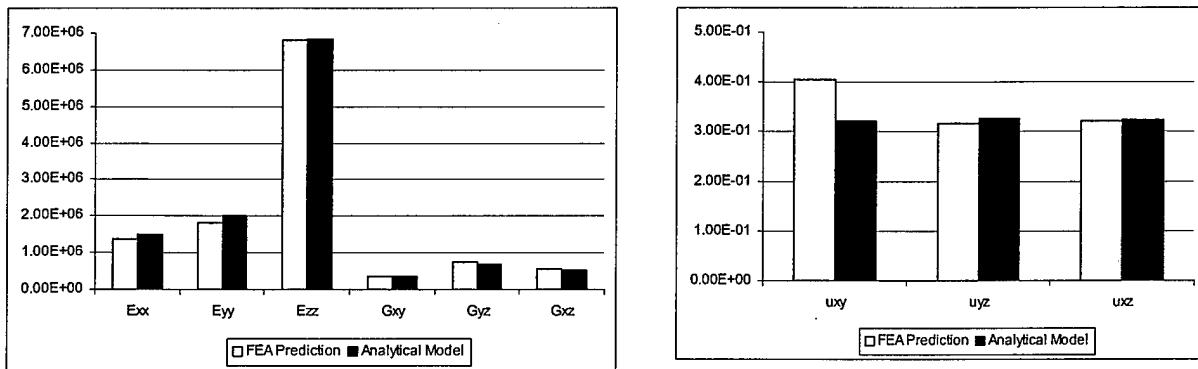

Figure 9. Comparison of FEA and analytical predictions (conducting core with cross section: 1 × 1.5 in, insulation layer thickness: 0.02 in, D = 0.3 in).

4.3 Parametric Studies

The effects of the fiber orientation in the composite layer and the change of the channel diameter on the effective properties of the conductor are studied, and the results are presented in Figures 10 and 11, respectively. It seems that the homogenized effective properties of the conductor are not sensitive to the fiber orientations, except for a slight variation for axial modulus, E_{ZZ}^{CC}, and the axial Poisson's ratio, v_{XZ}^{CC} and v_{YZ}^{CC}, as shown in Figure 10. The increase of the channel diameter will decrease the axial modulus, E_{ZZ}^{CC}, G_{XZ}^{CC}, and G_{YZ}^{CC}, as well as the transverse Poisson's ratio, v_{XY}^{CC}, but will produce less of an effect on the transverse modulus, E_{XX}^{CC}, E_{YY}^{CC}, and G_{XY}^{CC}, and has no effect on the axial Poisson's ratio, v_{XZ}^{CC} and v_{YZ}^{CC}, as shown in Figure 11. We believe that this trend of change is caused by the reduction of the axial modulus and the transverse Poisson's ratio of the metallic core due to the increase of the channel diameter.
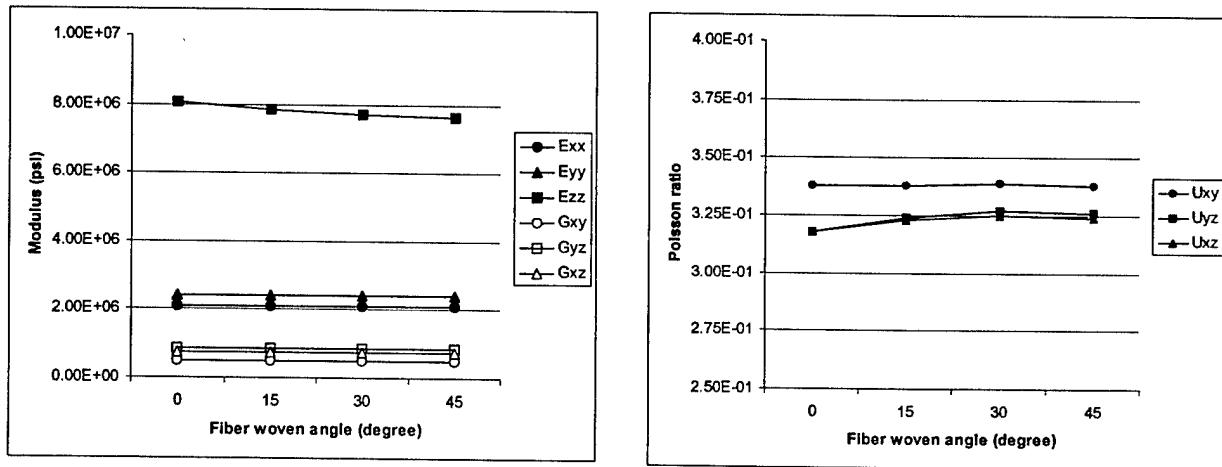

Figure 10. Effect of the plain-woven fiber orientation on the conductor effective properties (conducting core with cross section: 0.75 × 1.0 in, insulation layer thickness: 0.015 in, D = 0.3 in).

The variation of the conductor geometry, such as the change of the insulation layer thickness and change of the conductor core cross section on the effective properties of the conductor are also studied and the results are presented in Figures 12 and 13, respectively. It can be observed that the increase in the insulation layer thickness will, in general, decrease the effective modulus of the conductor because of the decrease of the conducting core volume. The three Young's modulus, E_{XX}^{CC}, E_{YY}^{CC}, and E_{ZZ}^{CC}, and the in-plane Poisson's ratio, v_{XY}^{CC}, are particularly sensitive to this change, while the shear modulus and the axial Poisson's ratios are less sensitive, as shown in Figure 12. Geometric variation, i.e., increasing the core height dimension, will affect the axial Young's modulus, E_{ZZ}^{CC}, and in-plane Poisson's ratio, v_{XY}^{CC}, but will not dramatically affect other conductor effective mechanical properties, as shown in Figure 13.
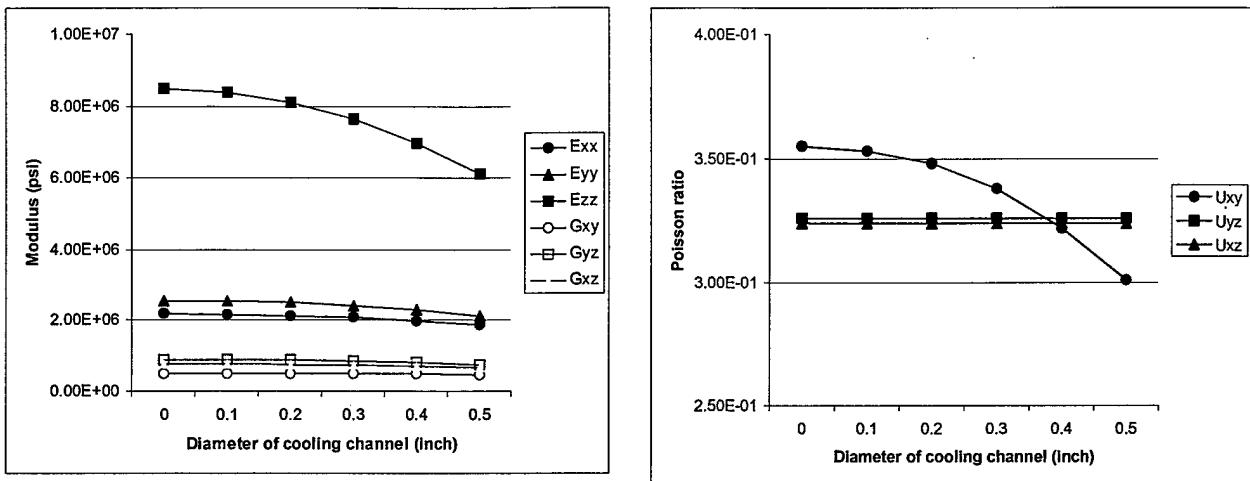
Figure 11. Effect of cooling channel diameter on the conductor effective properties (conducting core with cross section: 0.75 × 1.0 in, insulation layer thickness: 0.015 in).
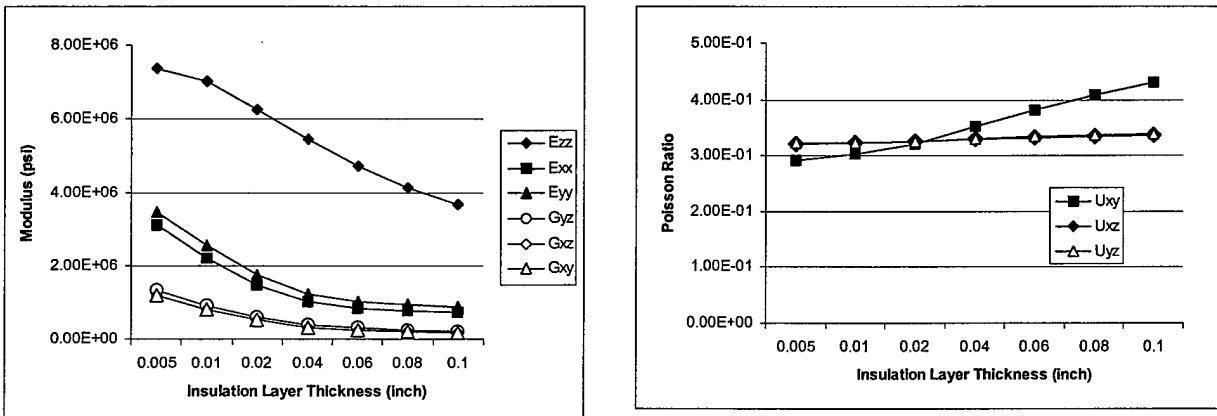
Figure 12. Effect of insulation layer thickness on conductor effective properties (conducting core cross section: 1 × 1.25 in, D = 0.3 in).

5. Summary and Conclusion

A homogenization modeling to predict the effective mechanical properties of EM composite conductor consisting of metallic core with cooling channel and insulating layers of different materials and ±θ° plain woven glass-fiber composite was presented. The homogenization scheme was developed based on the following two-level homogenization hierarchies: the homogenization of the metallic core with cooling channel and composite insulation blocks and the homogenization of the EM composite conductor. The CCAM was applied in the level 1

15
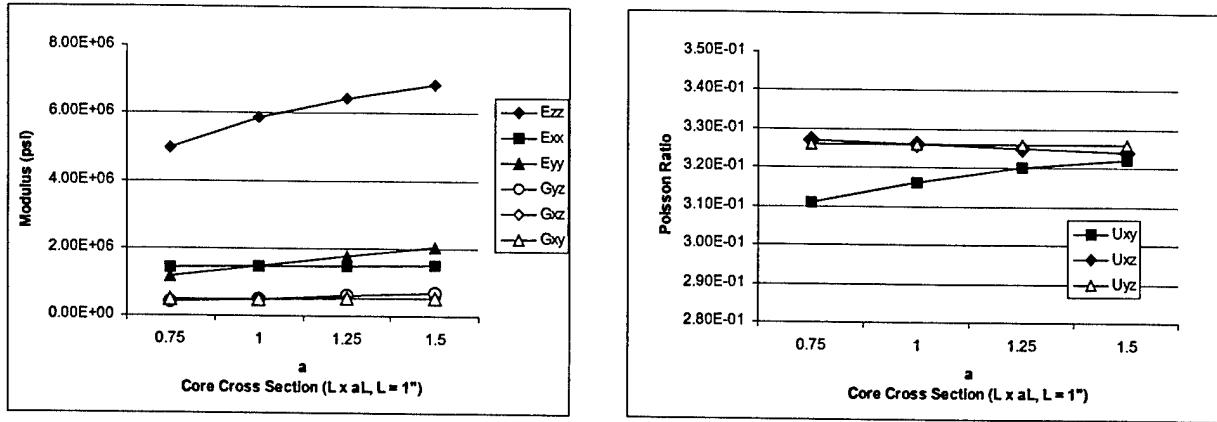
Figure 13. Effect of conducting core cross section on effective properties (conducting core cross section: L × aL with L = 1 in, insulation layer thickness = 0.02 in, D = 0.3 in).

homogenization process to derive the effective properties of the conducting core with the cooling channel. In the CCAM-based modeling, the cooling channel was analogized as a fiber void with null material properties. The effective mechanical properties of the composite insulation blocks were homogenized by smearing the properties of the insulating layers. In the derivation of the homogenization model to predict the effective mechanical properties of the composite conductor, combined sequences of the homogenization were used and the homogenization algorithms were executed based on either the displacement prescribed or the traction prescribed boundary conditions.

The developed homogenization model was applied to predict the effective mechanical properties of the EM composite conductor. The mechanical properties of the homogenized EM composite conductor behave anisotropically due to the material anisotropy and the structural anisotropy of the conductor. The material anisotropy is primarily caused by the constituent anisotropic properties of the insulation layer originated from the glass fiber plain-woven composite. The structural anisotropy is caused by the transverse dimensional difference in the conductor global structure. Both anisotropies contribute a significant difference between the transverse modules ($E_{XX}^{CC}, E_{YY}^{CC}, G_{XY}^{CC}$) and the axial modules ($E_{ZZ}^{CC}, G_{XZ}^{CC}, G_{YZ}^{CC}$), as shown in Table 2. The slight difference between E_{XX}^{CC} and E_{YY}^{CC} in Table 2 is due to the geometric difference of the conducting core in the X and Y directions, while this difference vanishes if the dimensions of the conducting core in X and Y are the same, as shown in Figure 13, where a = 1 for a conducting core with a square cross section. However, the effective Poisson's ratios of the conductor are not too sensitive to the material anisotropy and the structural anisotropy. There is no significant difference between the three principal Poisson's ratios, as observed in both Table 2 and in the subsequent figures. The good agreement between the analytical and numerical predictions as shown in Figures 8 and 9 demonstrates the applicability and accuracy of the developed homogenization model.

16

6. References

1. Fair, H. D., and E. M. Schmidt. "The Science and Technology of Electric Launch, A U.S. Perspective." *IEEE Transaction on Magnetics*, vol. 35, no. 1, pp. 11–18, 1999.

2. Walls, W. A., W. F. Weldon, S. B. Pratap, M. Palmer, and D. Adams. "Application of Electromagnetic Guns to Future Naval Platforms." *IEEE Transaction on Magnetics*, vol. 37, pp. 262–267, 1999.

3. Rosenwasser, S., G. Nagy, and G. Mehle. "The Design, Fabrication and Characterization of an Advanced Graphite Composite Structure for High Speed Rotating Machines." *IEEE Transaction on Magnetics*, vol. 35, no. 1, pp. 307–311, 1999.

4. Satapathy, S., and C. Persad. "Thermal Stress in EML Rail-Conductor Overlays." *IEEE Transaction on Magnetics*, vol. 37, no. 1, pp. 269–274, 2001.

5. Becherini, G., M. Raugi, and A. Tellini. "Thermal and Mechanical Stress in Induction Coilguns." *IEEE Transaction on Magnetics*, vol. 35, pp. 130–135, 1999.

6. Liu, H. P., Y. L. Ting, and R. C. Zowarka. "Electromagnetic and Structural Analyses of an Integrated Launch Package." *IEEE Transaction on Magnetics*, vol. 35, pp. 74–78, 1999.

7. Myatt, R. L., and P. H. Titus. "3D, Coupled Electromagnetic, Thermal, Current Diffusion in the Finger Joints of the Alcator C-Mod Toroidal Field Coils." *IEEE Transaction of Magnetics*, vol. 34, pp. 713–716, 1998.

8. Tzeng, J. T. "Mechanics of Composite Rotating Machines for Pulsed Power Applications." *IEEE Transaction on Magnetics*, vol. 37, no. 1, pp. 328–331, 2001.

9. Tzeng, J. T. "Dynamic Responses and Fracture of Composite Cylinders." *Journal of Composite Science and Technology*, vol. 58, no. 9, pp. 1443–1452, 1998.

10. Sun, W., and J. T. Tzeng. "Effective Mechanical Model of Electromagnetic (EM) Composite Conductor." ARL-TR-2674, U.S. Army Research Laboratory, Aberdeen Proving Ground, MD, February 2002.

11. Sun, W., and J. T. Tzeng. "Global-Local FEA Modeling for EM Composite Conductor With Cooling Channel." U.S. Army Research Laboratory, Aberdeen Proving Ground, MD, to be published.

12. Hashin, Z. "Theory of Fiber-Reinforced Materials." NASA-CR-1974, National Aeronautics and Space Administration, Washington, DC, 1974.

13. Huang, Z. M. "The Mechanical Properties of Composites Reinforced With Woven and Braided Fabrics." *Composite Science and Technology*, vol. 60, pp. 479–498, 2000.

14. Hill, R. "Elastic Properties of Reinforced Solids: Some Theoretical Principles." *Journal of the Mechanics and Physics of Solids*, vol. 11, pp. 357–372, 1963.

15. Hassani, B., and E. Hinton. "A Review of Homogenization and Topology Optimization I – Homogenization Theory for Media With Periodic Structure." *Computer & Structures*, vol. 69, pp. 707–717, 1998.

16. Hassani, B., and E. Hinton. "A Review of Homogenization and Topology Optimization II – Analytical and Numerical Solution of Homogenization Equations." *Computer & Structures*, vol. 69, pp. 719–738, 1998.

REPORT DOCUMENTATION PAGE

Public reporting burden for this collection of information is estimated to average 1 hour per response, including the time for reviewing instructions, searching existing data sources, gathering and maintaining the data needed, and completing and reviewing the collection of information. Send comments regarding this burden estimate or any other aspect of this collection of information, including suggestions for reducing this burden, to Washington Headquarters Services, Directorate for Information Operations and Reports, 1215 Jefferson Davis Highway, Suite 1204, Arlington, VA 22202-4302, and to the Office of Management and Budget, Paperwork Reduction Project(0704-0188), Washington, DC 20503.

1. AGENCY USE ONLY *(Leave blank)*	2. REPORT DATE	3. REPORT TYPE AND DATES COVERED
	November 2002	Final, October 2000–June 2002

4. TITLE AND SUBTITLE	5. FUNDING NUMBERS
Homogenization Modeling for Mechanical Properties of Composite Conductor With Cooling Channel	618622H.80

6. AUTHOR(S)

Wei Sun* and Jerome T. Tzeng

7. PERFORMING ORGANIZATION NAME(S) AND ADDRESS(ES)	8. PERFORMING ORGANIZATION REPORT NUMBER
U.S. Army Research Laboratory ATTN: AMSRL-WM-MB Aberdeen Proving Ground, MD 21005-5069	ARL-TR-2872

9. SPONSORING/MONITORING AGENCY NAMES(S) AND ADDRESS(ES)	10. SPONSORING/MONITORING AGENCY REPORT NUMBER

11. SUPPLEMENTARY NOTES

* ARL Research Associate under the Oak Ridge Institute for Science and Education program.

12a. DISTRIBUTION/AVAILABILITY STATEMENT	12b. DISTRIBUTION CODE
Approved for public release; distribution is unlimited.	

13. ABSTRACT *(Maximum 200 words)*

An electrical composite conductor may consist of a metallic core with a cooling channel and a multilayered insulating material. A model was developed to predict the mechanical properties of the composite conductor based on two-level homogenization hierarchies. A composite cylinder assembly model was developed in the level 1 homogenization for metallic core with a cooling channel, in which the cooling channel was analogized as a fiber void with null material properties. The effective mechanical properties of the composite insulation layers were homogenized by smearing the properties of the multiple polymer coatings and fiber-reinforced composite. In the level 2 homogenization, combined homogenization sequences were used based on the requirement of the displacement- or the traction-prescribed continuity. The developed model can calculate the nine effective mechanical constants of the conductor made of a metallic core and any angle ($\pm\theta°$) plain-woven glass-fiber composite. The model predictions were compared well with the results obtained from the finite element analyses. The developed model provides a theoretical basis and an accurate calculation for effective mechanical constants that are often difficult to be accurately determined through an experimental approach due to the structural heterogeneity and material anisotropy of the composite conductor.

14. SUBJECT TERMS		15. NUMBER OF PAGES
composite, homogenization, electromagnetics, conductor, armature, coil		24
		16. PRICE CODE

17. SECURITY CLASSIFICATION OF REPORT	18. SECURITY CLASSIFICATION OF THIS PAGE	19. SECURITY CLASSIFICATION OF ABSTRACT	20. LIMITATION OF ABSTRACT
UNCLASSIFIED	UNCLASSIFIED	UNCLASSIFIED	UL

NSN 7540-01-280-5500

Standard Form 298 (Rev. 2-89)
Prescribed by ANSI Std. 239-18   298-102

INTENTIONALLY LEFT BLANK.